Additive Manufacturing 79 (2024) 103916

Contents lists available at ScienceDirect

Additive Manufacturing

journal homepage: www.elsevier.com/locate/addma

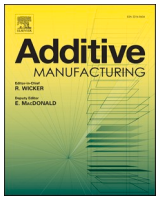

3D printing of photocatalytic nanocomposites containing titania nanoparticles

Roberto Bernasconi *, Umberto Bellè, Stefano Brigatti, Maria Vittoria Diamanti

Dipartimento di Chimica, Materiali e Ingegneria Chimica "Giulio Natta", Politecnico di Milano, via Mancinelli 7, 20131 Milano, Italy

ARTICLE INFO

Keywords:
Titanium dioxide
3D printing
Stereolitography
Composite
Photocatalysis

ABSTRACT

Titanium dioxide is a semiconductor ceramic material presenting notable electronic and physico-chemical properties. Its anatase form is characterized by excellent photocatalytic properties in presence of UV light, which justify its use for pollutants degradation or for the realization of self-cleaning surfaces. The potential of titania can be further valorized by integrating its unique properties in 3D printed parts and the most promising technology to do this, in consideration of its high resolution and flexibility, is vat photopolymerization. In the present work, titania/polymer composites are 3D printed using this technology and the resulting materials, containing nominal titania amounts up to 10% wt., are characterized from the morphological, microstructural and mechanical point of view. In addition, their photocatalytic activity is evaluated by performing Rhodamine B degradation tests under UV light. The composites showed remarkable activity levels, with a rate constant higher than 0.25 h^{-1} for the composite containing 10% wt. titania. Activity was increased by a local enrichment of TiO_2 in correspondence of the surface, resulting from the 3D printing process, and by a partial degradation of the polymer present between the titania particles in proximity of the surface.

1. Introduction

Thanks to its unique properties, titanium dioxide is one of the most studied functional materials in current applied research. Titania, indeed, is a n-type semiconductor characterized by a remarkable activity for heterogeneous photocatalysis [1,2] under UV light. This consideration is especially true for the anatase form, which presents the highest activity towards oxidation reactions [3]. As a consequence, anatase-rich titania has attracted broad interest for a wide range of applications, including the photodegradation of contaminants in water [4,5] and air [6,7], as well as the production of self-cleaning surfaces [8], antibacterial coatings [4,9] and of sensors [10]. Titania can be also easily doped [11], allowing these applications also under visible light illumination.

In general, titania can be applied to a surface in the form of thin film or as nanoparticles embedded in a composite. TiO_2 thin films can be deposited via magnetron sputtering [12], spin coating [13], dip coating [14], pulsed laser deposition [15] or chemical vapor deposition [16]. If the surface of interest is made of titanium, a peculiar way to form a layer of photoactive titania can be anodization [17]. In the case of composites, titania nanoparticles are normally codeposited with a matrix, which can be metallic or polymeric. Metallic based composites can be advantageously obtained by electrolytic [18–20] or electroless codeposition [21], whereas polymeric matrix materials can be deposited via casting [22], spraying [23] or spin coating [24]. An alternative approach to the deposition of photocatalytic films is the direct realization of the desired part with a bulk composite containing titania nanoparticles. This option presents interesting advantages if the titania bearing composite is manufactured using non-standard fabrication technologies.

One of the most attractive of these technologies, potentially capable of manufacturing parts made of titania loaded polymeric nanocomposites, is 3D printing (also known as additive manufacturing) [25]. The advantages of this family of techniques over conventional subtractive manufacturing are widely acknowledged: optimal material usage, less design constrains, possibility to obtain previously unattainable shapes, low cost, rapidity, high customizability of the final geometry. A technique in particular, vat photopolymerization [26], finds wide applicability when, in addition to the advantages previously enumerated, the final application also requires high dimensional accuracy, low porosity and reduced feature size. Clearly, all these attractive features can be combined with the photocatalytic properties of titania by loading the polymers used in 3D printing techniques like fused deposition modelling (FDM) or stereolithography (SLA) with TiO_2 nanoparticles.

* Corresponding author.
E-mail address: roberto.bernasconi@polimi.it (R. Bernasconi).

https://doi.org/10.1016/j.addma.2023.103916
Received 6 June 2023; Received in revised form 11 November 2023; Accepted 4 December 2023
Available online 7 December 2023

Indeed, many examples of additively manufactured composites combining the properties of two or more materials are available in literature [27–31]. The same is true for titania-based composites, which have been manufactured using mainly FDM, Direct Ink Writing (DIW) and SLA. Dolganov et al. investigated the DIW printability of a titania slurry [32]. Also Elkoro et al. used DIW and they manufactured monolithic structures that showed a significant photocatalytic activity [33]. McQueen et al. used FDM to print a highly photoactive polylactic acid – titania composite, which proved effective in the abatement of pollutants in water [34]. For what concerns SLA, printing attempts of composites have been carried out by Ávila-López et al. [35], Kozlov et al. [36] and Mubarak et al. [37], which did not evaluate their photocatalytic activity though. Finally, an interesting approach to get SLA 3D printed parts is the one reported by Vyatskikh et al. [38], who SLA printed a resin containing a dissolved titanium organocompound and pyrolized the resulting green part. By doing this, they achieved photoactive objects.

The aim of the present work is to investigate the applicability of digital light processing (DLP), a vat polymerization technique similar to SLA, to the 3D printing of a polymer based composite containing different nominal amounts of titania (2.5, 5 or 10% wt.) and to evaluate its photocatalytic properties as a function of the amount of TiO_2 embedded. The printability of the composite and its rheological properties are evaluated as a necessary prerequisite for the 3D printing tests. The morphology and phase composition of the printed composites is studied using scanning electron microscopy (SEM) and X-rays diffraction (XRD). Finally, water purification properties of the DLP printed titania nanocomposites are investigated for the first time by evaluating the photodegradation of the model molecule rhodamine B.

2. Experimental methods

2.1. Preparation of the TiO_2 loaded DLP resins

Degussa P25 titania nanoparticles were acquired from Evonik-Degussa. A general-purpose clear UV resin (Standard Clear resin, manufactured by Anycubic, 405 nm reticulation wavelength, density 1100 Kg m^{-3}; tensile strength 23.4 MPa) for SLA/DLP was acquired and used as received. The TiO_2 nanoparticles were dispersed in the resin in three different concentrations (2.5%, 5% and 10% wt.), stirred for 1 h and dispersed using a probe sonicator (model TU-900Y by Toption Group Co.). The dispersion process was carried out by directly immersing the 6 mm stainless steel probe into the solution under mechanical stirring, at 70% of the maximum power, applying 2 s on + 2 s off pulses for 10 min.

2.2. 3D printing process

The composites were 3D printed using a commercial DLP printer (Photon S by Anycubic). Step size was fixed to 50 μm and exposure time was tuned according to penetration depth. The latter was measured by exposing a single layer without building plate and then measuring its thickness by means of a micrometer. Square test samples were 3D printed using the clear resin and the three composites. Their dimensions were the following: 15 mm × 15 mm × 2 mm. Four bottom layers were printed, with an exposure time of 240 s. The 2.5% wt. TiO_2 composite was also used to print a grid (having external dimensions equal to 15 mm × 15 mm × 2 mm and presenting square pores of 2 mm × 2 mm). The 10% wt. TiO_2 composite was also used to print a complex geometry (the statue of an owl).

2.3. Characterization techniques

The rheological properties of the dispersions were assessed using a rotational rheometer (MCR 302 by Anton Paar). The viscosity tests were carried out using a parallel-plate configuration, with a diameter of the plates equal to 25 mm and a working gap equal to 1 mm. The irradiance of the screen present in the DLP printer was measured by means of a UV radiometer model UM-10 by Konica-Minolta. FT-IR characterization of the SLA resin was carried out using a Nicolet 380 instrument by Thermo-Fisher. Optical microscopy characterization was done using a DMLM microscope by Leica. SEM measurements were carried out by means of an EVO 50 EP setup by Zeiss, equipped with an Inca Energy 200 EDS unit by Oxford Instruments. The thermogravimetric analysis (TGA) was performed using a setup model STA 6000 by Perkin Elmer. The same instrument also yielded data of differential scanning calorimetry (DSC). XRD data were obtained using a diffractometer PW 1830 by Philips, equipped with a vertical goniometer PW 1820. The system worked in Bragg-Brentano configuration, exploiting the Cu K-α radiation. A HCV setup by Fischerscope, equipped with a Vickers diamond tip, was used for the microindentation tests.

2.4. Photocatalysis tests

Samples photocatalytic activity was tested in the degradation of a model organic dye, rhodamine B, in an aqueous solution. This is a widely diffused testing procedure in literature, which may allow a direct comparison of photocatalytic activity with previous works, allowing to better benchmark the materials produced with respect to the current state of the art [39,40]. Samples were suspended in beakers containing 40 mL of a 10^{-5} M aqueous solution of rhodamine B. Below the samples, a magnetic stirrer allowed solution homogenization throughout the test. UV irradiation was provided by a UV-A LED (Nichia NCSU033B, $\lambda_{radiation\ peak}$ = 365 nm, UV-A intensity = 11.1 mW/cm^2, Tokushima, Japan) positioned at a distance of 3 cm from the samples. Dye discoloration was evaluated by measuring dye absorbance every 1 h with a spectrophotometer SPECTRONIC 200E (Thermo Fisher Scientific, Les Ulis, France). The main absorption peak of the dye, at 555 nm, was employed and dye concentration was derived using the Beer–Lambert law [41]. Considering the pseudo-first order kinetics typical of dye degradation reactions [41], the kinetic constant can then be calculated as reported in Eq. 1.

$$\ln\frac{C}{C_0} = -k\ln t \tag{1}$$

where C is dye concentration at time t, C_0 its concentration at time zero, and k the rate constant. Tests were repeated multiple times on the samples. Tests were also performed in dark to verify possible dye concentration variations due to adsorption of the dye by the samples, and under UV-A LED in absence of the sample to evaluate photolysis, two phenomena that may alter dye concentration in solution, adversely influencing the reliability of actual degradation results. Eventually, the adsorbed dye was allowed to desorb to evaluate samples regeneration ability. The procedure involved the same setup of the photocatalysis test, exception made for the immersion solution, which was tap water with no rhodamine B addition.

3. Results and discussion

3.1. Chemical characterization of the resin

As first step of the experimentation, the chemical nature of the resin employed was determined. The clear UV resin is a proprietary formulation and the details of its composition are not available. In order to give some general indications about the chemistry of the material, however, FT-IR was carried out on two specimens (Fig. S1), one pristine and the second photopolymerized. The molecular fingerprint region of the spectra, magnified in Fig. S2, shows the typical features of an acrylate-based polymer [42]. Indeed, the peaks related to the $CH{=}CH_2$ in plane (1408 cm^{-1}) and out of plane (810 and 988 cm^{-1}) bend are of particular interest, since they totally disappeared in the photoreticulated resin, suggesting that the reactivity of the monomer is centered on a $CH{=}CH_2$ bond, as in the case of acrylates. Other relevant features present in the spectra are the C-O stretch (1072, 1117, 1200 and

1276 cm^{-1}), the C═C stretch (1640 cm^{-1}) and the C═O stretch (1725 cm^{-1}).

3.2. Composite printability evaluation

Once determined the nature of the resin, the composites were prepared by dispersing the TiO_2 nanoparticles in predetermined amounts and the stability of the resulting dispersions was qualitatively evaluated by sedimentation. A standard amount of material, 12 mL, was placed in glass vials and stored in dark for 24 h. At the end the dispersion maintained its uniformity (Fig. S3), with no sign of sedimentation. In fact, no deposit was found on the vial bottom and no relevant compositional differences were detected in the dispersion withdrawn from the top part of the fluid.

Following this preliminary stability assessment, the viscosity of the titania dispersions was measured and compared with the limits of the DLP machine here employed. Fig. 1a depicts the results of the rheological characterization of the materials, performed applying shear rates between 0.1 and 10,000 s^{-1}. The clear resin evidenced a mild non-Newtonian behavior, characterized by a shear-thinning nature. The materials containing titania nanoparticles, conversely, were considerably non-Newtonian. From the DLP point of view, acceptable viscosity ranges are mainly determined by the time required by the resin to flow under the build plate after each printing step. Indeed, between the curing of each layer, the resin must efficiently flow and perfectly fill the gap created by the movement of the plate. The movement of the plate normally happens at relatively low speeds, and low shear rates must be considered accordingly. Chen et al. [43] and Schwentenwein et al. [44] indicate, as acceptable viscosity for a successful DLP process, a value of 2×10^4 mPa s at shear rates between 10 and 100 s^{-1}. If this reference value is compared with the data reported in Fig. 1a, it appears evident that all the dispersions hereby described are fully printable.

Following the initial assessment of its properties, the actual printability of the dispersions was investigated by performing photopolymerization tests in the DLP printer. In detail, the clear resin and the three composites were photoreticulated at increasing exposure times (t_e) in order to estimate the dependence of the curing depth (C_d) on the energy provided to the material (Fig. 1b). Indeed, the curves present an exponential trend, as typically observed in these tests. The UV radiation blocking effect of titania can be clearly observed, as the curves shift

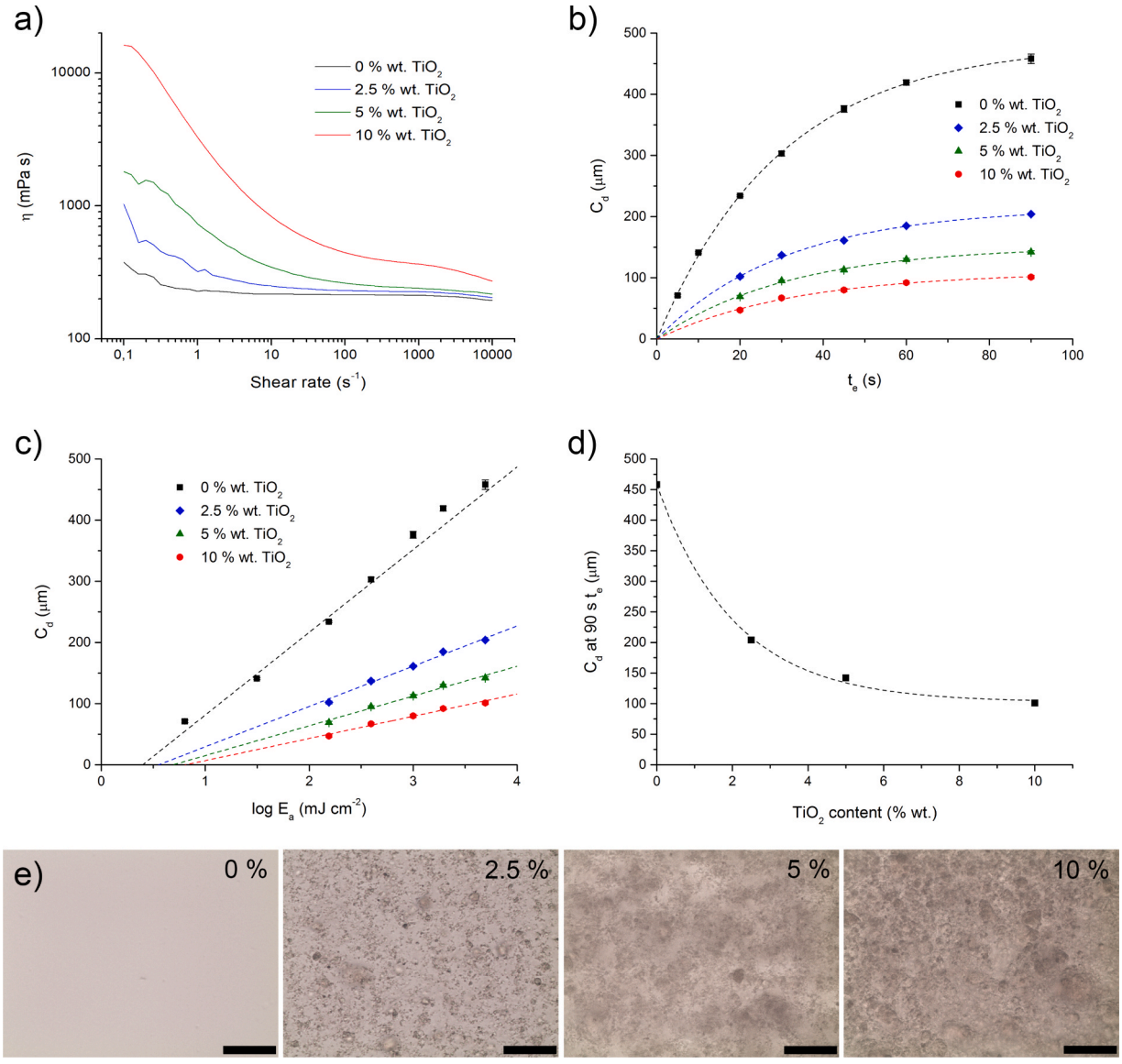

Fig. 1. Rheological characterization of the composites (a); time-dependent photoreticulation curves for the DLP printing of the composites (b); energy-dependent photoreticulation curves for the DLP printing of the composites (c); curing depth dependance from titania content of the composites (d); optical microscope images of the DLP printed composites (e, scalebar 20 µm).

towards lower values of C_d at increasing contents of titania. Indeed, the presence of titania strongly decreases the intensity of the radiation that penetrates the material, and consequently decreases the depth of the cured zone (at constant t_e). The effect is visualized in Fig. 2d, where the C_d for the four materials is reported for a constant t_e of 90 s. By adding increasing amounts of titania, the value of C_d exponentially decreased and it became 44.5% of the value observed for the clear resin in the case of the 2.5% wt. TiO_2 composite, 31% for the 5% wt. TiO_2 composite and 22.1% for the 10% wt. TiO_2 composite.

The printability of the composites can be evaluated in a more rigorous way by considering the energy per unit area provided to the material. This can be calculated multiplying t_e for the power per unit of area measured on the screen of the LCD printer. The latter was measured by means of a photometer, obtaining a value of 0.447 ± 0.015 mW/cm^2. As reported by Bennett et al. [45], the relationship between the logarithm of the energy density provided to the material (E_a) and C_d is expected to be linear (Eq. 2).

$$C_d = D_p \quad \ln\frac{E_a}{E_c} \tag{2}$$

The two parameters D_p and E_c are known as depth of penetration and critical energy, respectively. These are constants typical of each material and represent the sensitivity of the material itself to a variation of the energy provided (D_p) and the minimum amount of energy required to start the photopolimerization (E_c). Considering Eq. 1, data reported in Fig. 2a were replotted and linearly fitted, obtaining the graph presented in Fig. 1c. The corresponding fitting parameters are reported in Table 1.

As expectable, the composites require higher values of E_c to start polymerization as the titania loading increases. Furthermore, they become progressively less sensitive to the variation of energy density

Table 1
Fitting parameters for curing depth data linear regression.

Material	D_p	E_c (mJ cm^{-2})
Clear resin	135.19	2.49
2.5% wt. TiO_2	65.87	3.56
5% wt. TiO_2	48.67	4.89
10% wt. TiO_2	36.26	6.47

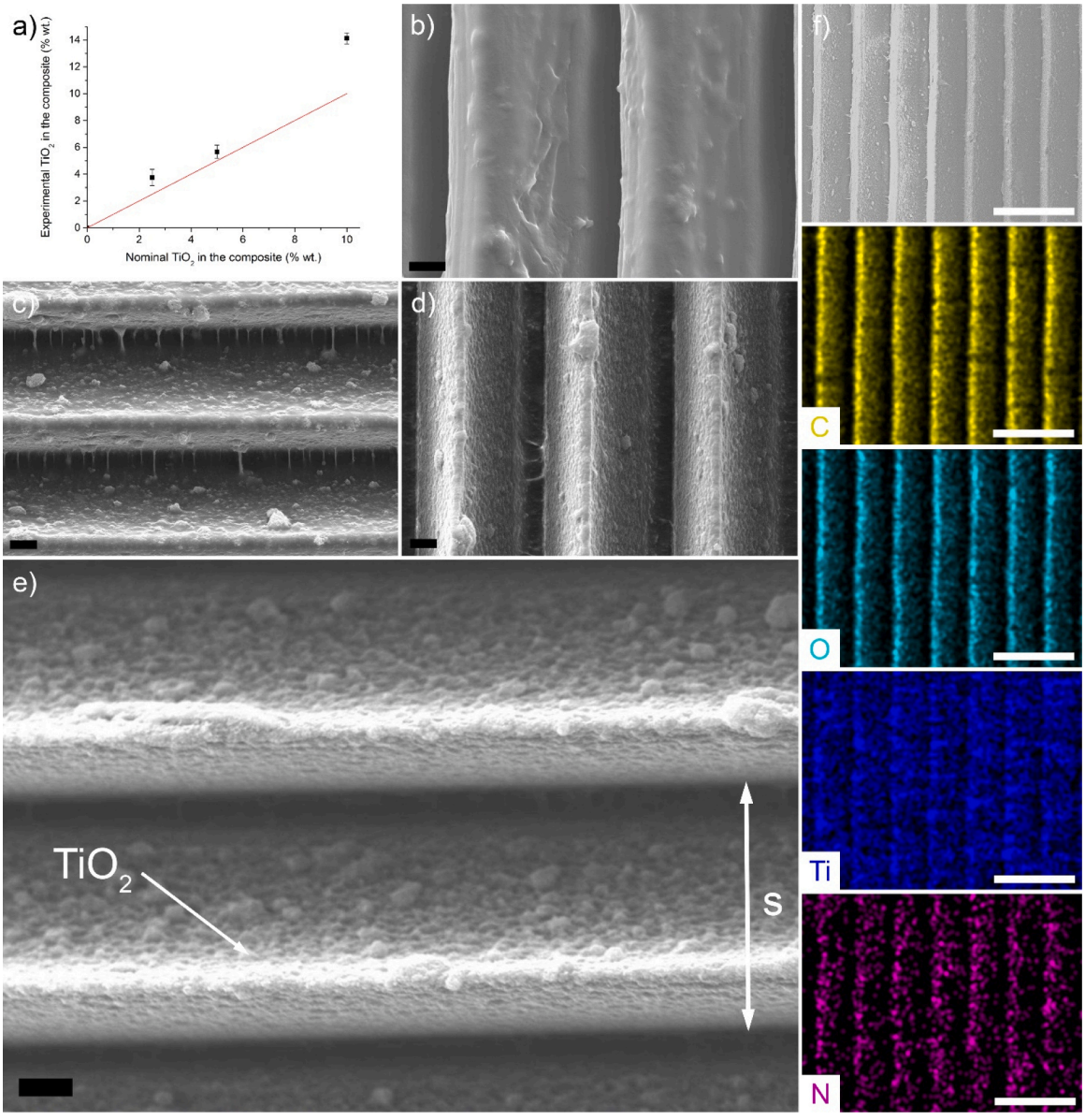

Fig. 2. Nominal vs. experimental TiO_2 content for the composites (a); SEM morphology of the 0% wt. TiO_2 (b, scalebar 10 μm), 2.5% wt. TiO_2 (c, scalebar 10 μm), 5% wt. TiO_2 (d, scalebar 10 μm), 10% wt. TiO_2 (e, scalebar 10 μm) composites; EDS elemental mapping for the 10% wt. TiO_2 composite (f, scalebar 100 μm).

(their penetration depth decreases).

Regardless the progressive loss of photosensitivity recorded in the presence of titania, all dispersions were found to be fully printable with the t_e values appropriate for the step height employed, which was set to 50 μm for all samples produced. The values of t_e employed were the following: 8 s for the clear resin, 20 s for the 2.5% wt. TiO_2 composite, 30 s for the 5% wt. TiO_2 composite, 40 s for the 10% wt. TiO_2 composite. Under these conditions, 4 layers (for a total of 200 μm) were printed for each material employed to evaluate the dispersion of the TiO_2 nanoparticles in the photopolymerized composite. Fig. 1e depicts the result obtained, observed at the optical microscope. Images clearly evidence an increasing amount of titania nanoparticles moving from the 0% wt. sample to the 10% wt. sample. In all cases, titania appears relatively agglomerated into aggregates.

3.3. Characterization of the 3D printed titania composites

In order to study the properties of the photoreticulated resins, square test samples were 3D printed (Figs. S4 and S5). Their elemental composition was evaluated during SEM observations, when EDS was used to verify the TiO_2 content (Fig. 2a). All samples present on the surface, in the few micrometers analyzable by the instrument, a titanium concentration higher than the nominal one (represented by the red line in Fig. 2a). This surface enrichment has already been observed in the case of SLA printed parts [46] and results beneficial for the photocatalytic properties of the 3D printed part.

Also the morphology of the square test samples was characterized using SEM (Fig. S6 and figures from 2b to 2e). In general, samples present the typical step-like morphology of DLP printed parts. The height of each step corresponds to the step size *s* selected (in this case, 50 μm) and their presence is connected to the interactions taking place between the resin and the UV light generated by the screen of the printer. Indeed, the resin partially scatters UV light, resulting into an overcuring that yields the steps visible in Fig. S6 (clear resin sample). Fig. 2b shows the same sample observed at higher magnification. The clear resin presents a relatively flat morphology at the micrometric scale. When TiO_2 concentration increases, on the contrary, roughness progressively increases. This is evident by comparing Fig. 2c (2.5% wt. titania), Fig. 2d (5% wt. titania) and Fig. 2e (10% wt. titania). In addition, the steps between each printed layer appear more pronounced when titania content increases. This is somewhat expectable, as titania considerably increases the scattering of UV radiation [47], thus enhancing the overcuring effect already observed in the clear resin. Fig. 2f shows the elemental mapping (for C, O, Ti and N) of the 10% wt. TiO_2 composite. The Ti signal, linked to the presence of titania, appears relatively uniform on the surface, indicating thus a good uniformity in the dispersion of titania itself.

Fig. 3a shows the cross section of a 10% wt. TiO_2 sample. The considerable height of the overcured region suggests a strong scattering interaction between titania and UV light. In order to demonstrate the possibility to print more complex structures, the grid visible in Fig. S7 was 3D printed using the 10% wt. composite. Printing supports were employed (Fig. S8) in order to print the grids with a moderate tilting with respect to the build plate. Fig. 3b depicts the SEM morphology of such grid. A partial overcuring inside the pores, which is expectable for a material that presents a high scattering for the UV radiation, can be observed. The presence of pronounced overcured zones can be appreciated in Fig. 3c. Fig. 3d, on the contrary, offers the possibility to observe the morphology of the titania aggregates present in the composites. Indeed, the high magnification employed to acquire Fig. 3d makes possible the observation of round shaped nanometric aggregates partially buried in the resin or protruding from the surface. This material, due to its position at the interface, is the most active from the photocatalytic point of view.

In addition to the grids, also a complex geometry was 3D printed to demonstrate the potentiality of the materials hereby described. In detail,

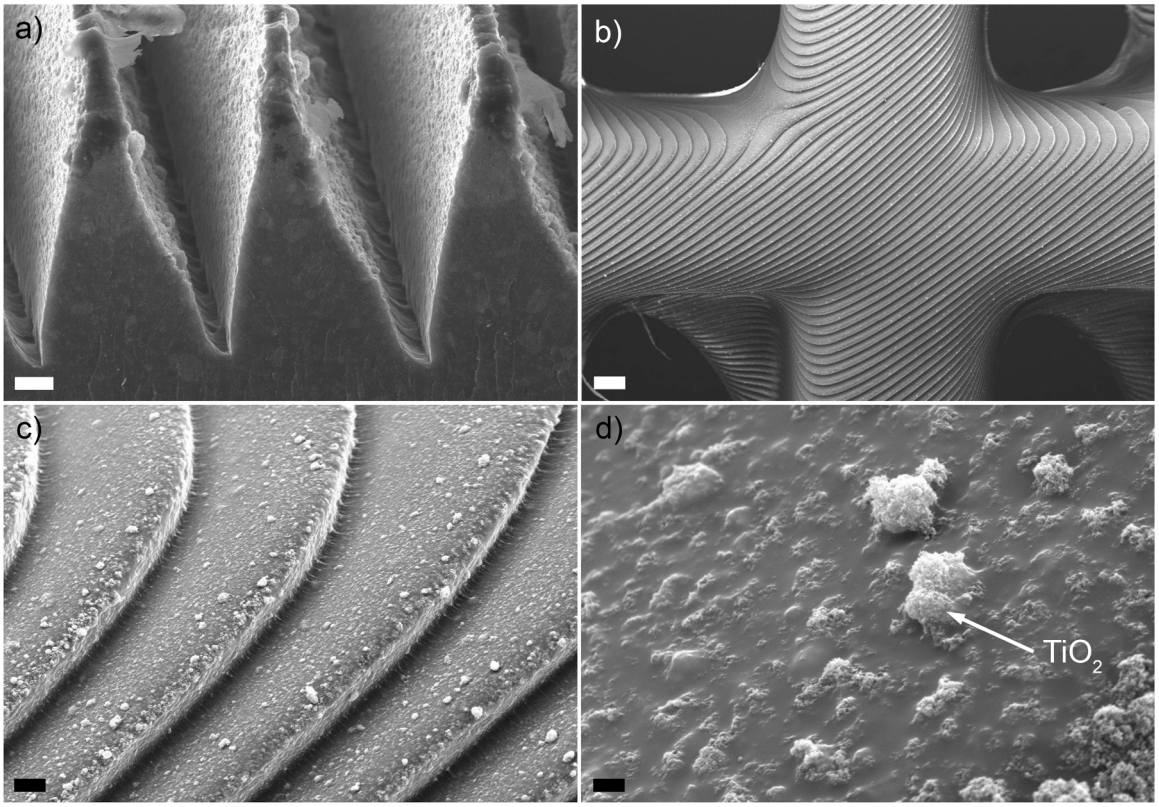

Fig. 3. SEM cross section of a 10% wt. composite (a, scalebar 10 μm); SEM morphology of a DLP printed grid observed at 100 X (b, scalebar 200 μm), 1000 X (c, scalebar 20 μm) and 10000 X (d, scalebar 2 μm).

the 3D model reported in Fig. S9 was 3D printed, obtaining thus the owl statue visible in Fig. S10.

The characterization of the 3D printed materials was completed by evaluating their thermogravimetric behavior, their phase composition and their mechanical properties. The first was studied using TGA (Figs. 4a, 4b). As expectable, the terminal mass at 900 °C for the composites almost exactly corresponded to the nominal amount of TiO_2 loaded (Fig. 4a). In particular, it was 0.07% wt. for the 0% wt. composite, 2.75% wt. for the 2.5% wt. composite, 5.05% wt. for the 5% wt. composite and 9.6% wt. for the 10% wt. composite. All composites evidenced a first loss of weight around 100 °C, which was probably due to water loss, and a second around 200 °C (Fig. 4b). The latter was realistically correlated to a loss of uncured monomer. Table 2 reports the values for the weight losses (ΔW) observed at 100 °C and 200 °C for the different composites.

The weight loss observed in the 30–100 °C range decreased by increasing the amount of titania in the composite, suggesting a decreasing tendency to adsorb water from the atmosphere. The weight loss recorded in the 100–200 °C interval, on the contrary, steadily increased by increasing the amount of titania. This suggests the present of increasing amounts of unreacted monomer in the composite as a consequence of the light shielding effect of the TiO_2 nanoparticles.

The TGA setup also provided a DLC signal, which is reported in Fig. S11. All the composites evidenced a variation in the heat flow around 120 °C, which may coincide with the evaporation of the unreacted monomer. In addition, a strong variation in the heat flow was observed for temperatures higher than 200 °C. This, together with the significant weight losses observable in Fig. 4a, indicates the degradation of the resin matrix present in the composites.

Table 2
Weight losses observed at 100 °C and 200 °C for the composites.

Material	ΔW 30–100 °C (% wt.)	ΔW 100–200 °C (% wt.)
Clear resin	0.845	0.707
2.5% wt. TiO_2	0.855	0.888
5% wt. TiO_2	0.633	1.065
10% wt. TiO_2	0.319	1.24

The phase composition of the materials was determined using XRD, whose results are reported in Fig. 4c. The clear resin was found to be substantially amorphous, with a broad peak around 20°. Samples containing titania show sharp peaks superimposed to the amorphous background of the resin. These peaks corresponds to the positions of titania [48] in the form of anatase (JCPDS card 00–021–1272) and rutile (JCPDS card 01–070–7347), and their intensity progressively increased with the amount of titania present in the composite. Degussa P25 titania normally contains 70–80% anatase and 20–30% rutile. This ratio was qualitatively present also in the composites.

Finally, the hardness and the elastic modulus *E* of the composites were evaluated performing Vickers microindentation tests (Fig. 4d). With respect to the clear resin, the composites systematically presented lower values for hardness and elastic modulus. The 10% wt. titania composite, for example, was characterized by a value of Vickers hardness that was only 26.5% of the value observed for the unloaded resin. A similar consideration can be done in the case of *E* (48%). TiO_2, by significantly scattering UV light, realistically prevents the complete reticulation of the resin. This consideration is supported by the amounts of unreacted monomer observed in titania containing composites

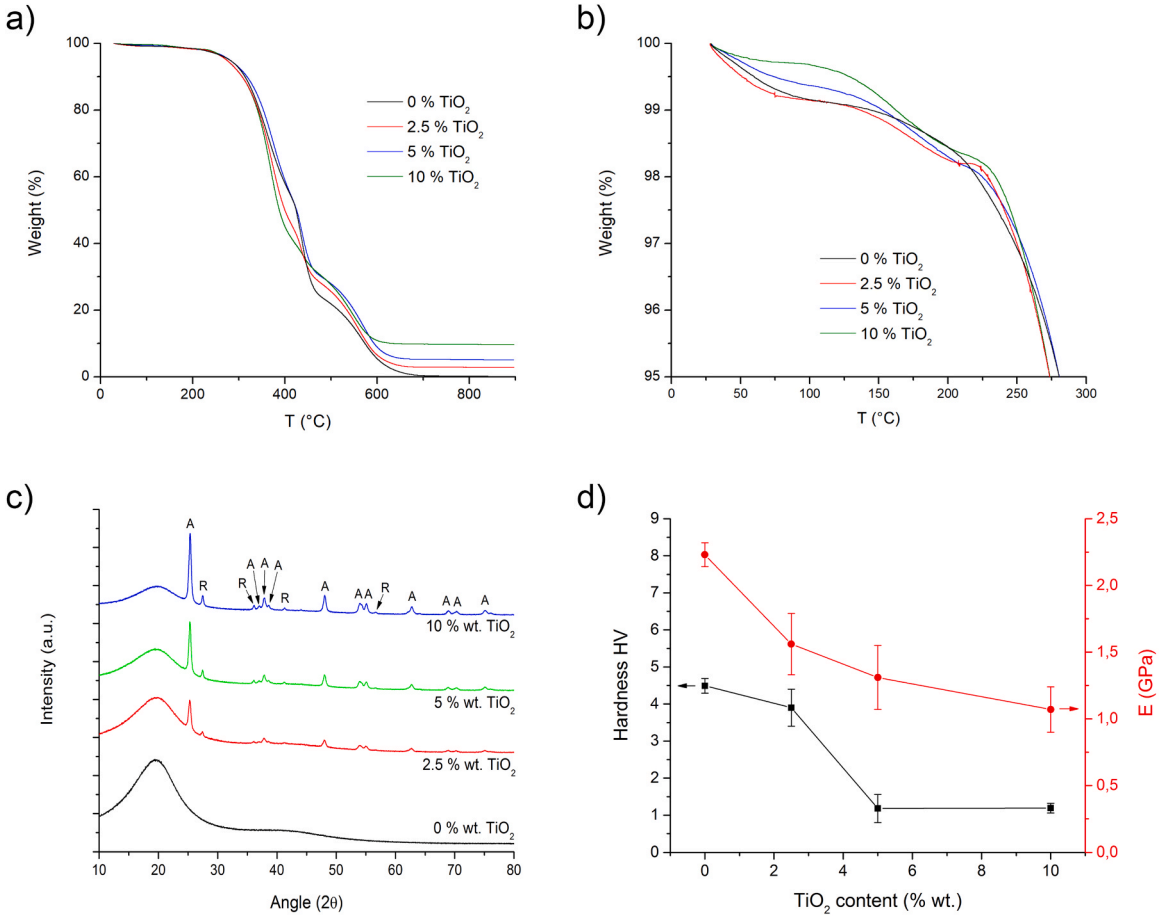

Fig. 4. TGA characterization of the DLP printed composites (a and b); XRD characterization of the DLP printed composites (c); mechanical characterization of the DLP printed composites (d).

(Table 2). The final outcome of this lower monomer conversion are decreased mechanical properties, in analogy with what observed by Bustillos et al. [49].

3.4. Photocatalysis tests

Both full samples and the grid sample were then tested for photocatalytic activity. Several aspects were considered: the overall disappearance of rhodamine B (RhB) from the aqueous solution, which was quantified as variation in absorbance; the disappearance only due to adsorption on the samples surfaces, without photoactivation; and photolysis, in presence of the same UV light used in tests but without sample. While the latter was negligible, due to the high refractoriness of RhB towards degradation, adsorption was evident, as samples immersed in solution changed color from white to pink. Still, the amount of dye adsorbed was sufficient to provoke surface coloring, but did not alter significantly the solution absorbance, therefore its possible alteration on photocatalytic tests results was considered negligible as well. For example, the variation of absorbance observed after 6 h in the dark for a 10% wt. TiO_2 sample was negligible. The samples color alteration will be further discussed in the following. In addition, the shape of the adsorption spectrum (Fig. S12) was also monitored to verify that no de-

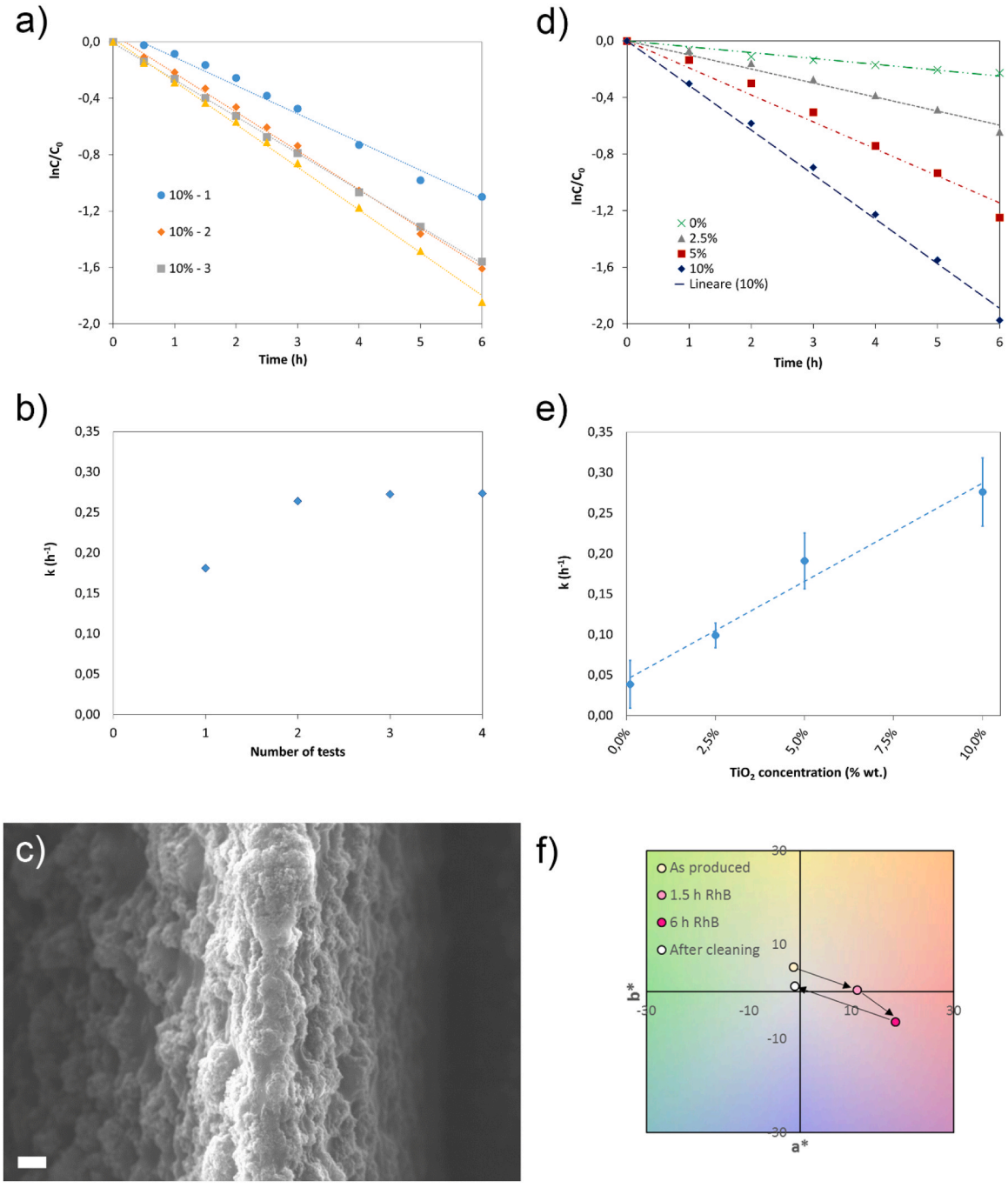

Fig. 5. Photocatalytic degradation of RhB from a sample with 10% wt. of TiO_2 (a); evolution over 4 photodegradation cycles of the rate constant for a 10% wt. TiO_2 sample (b); SEM of a sample containing 10% wt. TiO_2 after 4 cycles of irradiation (c); photocatalytic degradation of RhB from composites with increasing titania contents (d); dependence of the rate constant from titania content of the composites (e); color analysis of the samples before, during and after photocatalysis and cleaning (f).

ethylation occurred, which would only shift the peak to lower wavelengths without causing the dye conjugated structure degradation. Considering the results obtained, no relevant de-ethylation was observed.

In Fig. S13, tests performed on the sample with the highest TiO_2 loading (10% wt.) are reported. The same sample was used repeatedly, up to 4 tests. Absorbance variation is reported in Fig. S13, while Fig. 5a reports the $\ln C/C_0$ versus t graph, whose linear trend confirms the pseudo first order reaction kinetics, with a slope that corresponds to the rate constant. It is immediately clear that the material behavior changes after repeated tests. Indeed, the initial photoactivity is lower and it increases along multiple runs, with a marked increase after the first test and then only marginal variations. The variation in the photocatalytic activity of the composite can be efficiently visualized by plotting the values of k observed in the 4 consecutive tests (Fig. 5b). The presence of a plateau, reached at the third test, is clearly evident. A similar behavior was also observed at lower TiO_2 contents; for this reason, the following comparisons are made on samples subjected to 4 test runs, where the largest variations in photoactivity have already been obtained. The reason for this increasing photocatalytic activity must be sought in a partial degradation of the resin matrix, which led to TiO_2 being more exposed at the sample surface, and therefore to better photocatalytic activity: this can be seen in Fig. 5c, which reports an image of the surface after 4 cycles of irradiation. By comparing this image with the SEM image of the pristine surface (Fig. S14), no direct damages to the matrix (like cracks or fractures) are visible. However, it is possible to clearly see a rougher surface, due to the protrusion of TiO_2 nanoparticles from the partially degraded matrix.

Fig. 5d reports a comparison of the $\ln C/C_0$ data obtained from the samples with different additions of TiO_2, while Fig. 5e reports the corresponding values of photocatalytic reaction rates. A linear trend for the rate constant is observed with the TiO_2 content in the composite. The slight photoactivity observed in absence of TiO_2 is ascribable to a sum of photolysis and adsorption, which – even when put together – do not concur relevantly to photocatalytic degradation.

As anticipated, samples resulted pink after the tests. Color is represented in the CIELab space [50], as defined by the International Commission on Color, CIE (Commission Internationale de l'Éclairage), being a* the chromatic coordinate ranging from green (-a*) to red (+a*), b* the coordinate ranging from blue (-b*) to yellow (+b*), and L* the lightness. Fig. 5f represents the color of the samples and their variation before use, after short-term immersion in RhB in dark (1.5 h), after a full photocatalysis test (6 h) and after regeneration, which is performed by exposing the sample to UV light for 6 h in water. First of all, it is clear that the adsorption increases with time, as the color point moves towards more red hues and less yellow/more blue hues, i.e., its color turns toward that of the original RhB solution. It is also evident how regeneration completely restores the material surface, eliminating residual RhB. This is confirmed by photocatalysis tests repetitions as well, since the increasing activity observed in multiple repetitions would not be possible if the surface was saturated with RhB or its byproducts. On the other hand, the slight decrease in yellow coordinate observed between the beginning of the test and the end of regeneration, associated with a decrease in lightness, confirms the hypothesis of polymer degradation: indeed, acrylates have a yellowish component, while titanium dioxide is bright white, hence its exposure at the sample surface due to polymer degradation would lead to surface whitening, plus the consequent surface roughening would justify the decreased lightness on such a bright color.

4. Conclusions

The experimentation carried out demonstrates that titania-based composites presenting remarkable photocatalytic properties can be successfully 3D printed by means of DLP. TiO_2 nanoparticles can be effectively added to commercial acrylate based DLP resins, obtaining well dispersed and stable dispersions that evidence a good printability. The composites show an expectable overcuring tendency, but complex geometries presenting a uniform content of titania can be efficiently printed. The DLP printing process exhibits the tendency to locally enrich in TiO_2 the surface of the composites, which is beneficial from the photocatalytic point of view. Indeed, being photocatalysis a surface phenomenon, any local enrichment translates into an increase in activity. Beside the enrichment due to the DLP process, a further increase in surface titania concentration is recorded after a few photocatalysis tests. In fact, titania not only catalyzes the degradation of the pollutant present in solution, but also induces the partial degradation of the resin present between the TiO_2 nanoparticles. This effect, which shows a plateau after 3 photodegradation cycles, further enhances the activity of the composite. The combination of these two surface titania enrichment phenomena, the DLP-related and the photodegradation-related, translates into activity levels higher than the ones expectable for the nominal TiO_2 concentrations present in the composites. From the applicative point of view, the titania composites here presented can be potentially employed for the realization of 3D printed photodegradation reactors for water purification or to manufacture antibacterial/antifungal surfaces.

CRediT authorship contribution statement

Brigatti Stefano: Writing – original draft, Visualization, Investigation, Formal analysis. **Diamanti Maria Vittoria:** Writing – original draft, Validation, Supervision, Software, Resources, Project administration. **Bernasconi Roberto:** Writing – original draft, Validation, Methodology, Investigation, Conceptualization. **Bellè Umberto:** Writing – original draft, Visualization, Validation, Formal analysis, Data curation.

Declaration of Competing Interest

The authors declare that they have no known competing financial interests or personal relationships that could have appeared to influence the work reported in this paper.

Data Availability

Data will be made available on request.

Acknowledgements

The authors wish to thank Prof. Luca Magagnin (Politecnico di Milano) for providing his support to the project.

Appendix A. Supporting information

Supplementary data associated with this article can be found in the online version at doi:10.1016/j.addma.2023.103916.

References

[1] T. Parangi, M.K. Mishra, Titania nanoparticles as modified photocatalysts: a review on design and development, Comments Inorg. Chem. 39 (2019) 90–126.
[2] W.-N. Zhao, Z.-P. Liu, Mechanism and active site of photocatalytic water splitting on titania in aqueous surroundings, Chem. Sci. 5 (2014) 2256–2264.
[3] K. Yaemsunthorn, M. Kobielusz, W. Macyk, TiO2 with tunable anatase-to-rutile nanoparticles ratios: how does the photoactivity depend on the phase composition and the nature of photocatalytic reaction? ACS Appl. Nano Mater. 4 (2021) 633–643, https://doi.org/10.1021/acsanm.0c02932.
[4] M. Soleimani, J.B. Ghasemi, G.M. Ziarani, H. Karimi-Maleh, A. Badiei, Photocatalytic degradation of organic pollutants, viral and bacterial pathogens using titania nanoparticles, Inorg. Chem. Commun. 130 (2021), 108688.
[5] J. Carbajo, M. Jiménez, S. Miralles, S. Malato, M. Faraldos, A. Bahamonde, Study of application of titania catalysts on solar photocatalysis: Influence of type of pollutants and water matrices, Chem. Eng. J. 291 (2016) 64–73.

[6] A.H. Mamaghani, F. Haghighat, C.-S. Lee, Effect of titanium dioxide properties and support material on photocatalytic oxidation of indoor air pollutants, Build. Environ. 189 (2021), 107518.
[7] V. Seiß, S. Thiel, M. Eichelbaum, Preparation and real world applications of titania composite materials for photocatalytic surface, air, and water purification: state of the art, Inorganics 10 (2022) 139.
[8] N.T. Padmanabhan, H. John, Titanium dioxide based self-cleaning smart surfaces: a short review, J. Environ. Chem. Eng. 8 (2020), 104211.
[9] Z. Jing, D. Guo, W. Wang, S. Zhang, W. Qi, B. Ling, Comparative study of titania nanoparticles and nanotubes as antibacterial agents, Solid State Sci. 13 (2011) 1797–1803.
[10] J.M. Rzaij, A.M. Abass, Review on: TiO2 thin film as a metal oxide gas sensor, J. Chem. Rev. 2 (2020) 114–121.
[11] N. Kaur, S.K. Shahi, J.S. Shahi, S. Sandhu, R. Sharma, V. Singh, Comprehensive review and future perspectives of efficient N-doped, Fe-doped and (N, Fe)-co-doped titania as visible light active photocatalysts, Vacuum 178 (2020), 109429.
[12] P.J. Kelly, G.T. West, M. Ratova, L. Fisher, S. Ostovarpour, J. Verran, Structural formation and photocatalytic activity of magnetron sputtered titania and doped-titania coatings, Molecules 19 (2014) 16327–16348.
[13] A. Kompa, D. Kekuda, K. Mohan Rao, A comparative study on the structural, optical, and electrical properties of titania films grown by spin-coating method, Appl. Phys. A. 126 (2020) 1–9.
[14] D. Dastan, S.L. Panahi, N.B. Chaure, Characterization of titania thin films grown by dip-coating technique, J. Mater. Sci. Mater. Electron. 27 (2016) 12291–12296.
[15] J. Swaminathan, S. Ravichandran, P. Palani, M. Mathankumar, S. Balasubramanian, Probing the defect-driven tunable photo (electro) catalytic water-splitting behavior of pulsed-laser-deposited titania, Energy Fuels 35 (2021) 4512–4523.
[16] J.L. Hodgkinson, H.M. Yates, A. Walter, D. Sacchetto, S.-J. Moon, S. Nicolay, Roll to roll atmospheric pressure plasma enhanced CVD of titania as a step towards the realisation of large area perovskite solar cell technology, J. Mater. Chem. C. 6 (2018) 1988–1995.
[17] L. Razzaboni, M. Altomare, M. Pedeferri, M.V. Diamanti, P. Schmuki, Hierarchical anodic TiO2 nanostructures formed in ethylene Glycol/o-H3PO4 electrolytes for direct photocatalysis, ChemElectroChem 7 (2020) 2859–2863.
[18] V.S. Protsenko, A.A. Kityk, E.A. Vasil'eva, A.V. Tsurkan, F.I. Danilov, Electrodeposition of composite coatings as a method for immobilizing TiO 2 photocatalyst, in: Nanophotocatalysis Environ. Appl., Springer, 2019, pp. 263–301.
[19] R. Bernasconi, E. Carrara, M. Hoop, F. Mushtaq, X. Chen, B.J. Nelson, S. Pané, C. Credi, M. Levi, L. Magagnin, Magnetically navigable 3D printed multifunctional microdevices for environmental applications, Addit. Manuf. 28 (2019) 127–135.
[20] M. Poorraeisi, A. Afshar, The study of electrodeposition of hydroxyapatite-ZrO2-TiO2 nanocomposite coatings on 316 stainless steel, Surf. Coat. Technol. 339 (2018) 199–207.
[21] W.-T. Chiu, C.-Y. Chen, T.-F.M. Chang, T. Hashimoto, H. Kurosu, M. Sone, Ni–P and TiO2 codeposition on silk textile via supercritical CO_2 promoted electroless plating for flexible and wearable photocatalytic devices, Electrochim. Acta 294 (2019) 68–75.
[22] D. Lin, Y. Huang, Y. Liu, T. Luo, B. Xing, Y. Yang, Z. Yang, Z. Wu, H. Chen, Q. Zhang, Physico-mechanical and structural characteristics of starch/polyvinyl alcohol/nano-titania photocatalytic antimicrobial composite films, Lwt 96 (2018) 704–712.
[23] Y. Li, B. Luo, C. Guet, S. Narasimalu, Z. Dong, Preparation and formula analysis of anti-biofouling titania–polyurea spray coating with nano/micro-structure, Coatings 9 (2019) 560.
[24] X. Cui, G. Zhu, Y. Pan, Q. Shao, M. Dong, Y. Zhang, Z. Guo, Polydimethylsiloxane-titania nanocomposite coating: fabrication and corrosion resistance, Polym. (Guildf.) 138 (2018) 203–210.
[25] I. Gibson, D.W. Rosen, B. Stucker, M. Khorasani, Additive manufacturing technologies, Springer, 2021.
[26] P.J. Bártolo, Stereolithography: materials, processes and applications, Springer Science & Business Media, 2011.
[27] U. Kalsoom, P.N. Nesterenko, B. Paull, Recent developments in 3D printable composite materials, RSC Adv. 6 (2016) 60355–60371.
[28] I. Blanco, The use of composite materials in 3D printing, J. Compos. Sci. 4 (2020) 42.
[29] X. Wang, M. Jiang, Z. Zhou, J. Gou, D. Hui, 3D printing of polymer matrix composites: a review and prospective, Compos. Part B Eng. 110 (2017) 442–458.
[30] J. Saroia, Y. Wang, Q. Wei, M. Lei, X. Li, Y. Guo, K. Zhang, A review on 3D printed matrix polymer composites: its potential and future challenges, Int. J. Adv. Manuf. Technol. 106 (2020) 1695–1721.
[31] A. Al Rashid, W. Ahmed, M.Y. Khalid, M. Koc, Vat photopolymerization of polymers and polymer composites: Processes and applications, Addit. Manuf. 47 (2021), 102279.
[32] A. Dolganov, M.T. Bishop, G.Z. Chen, D. Hu, Rheological study and printability investigation of titania inks for Direct Ink Writing process, Ceram. Int. 47 (2021) 12020–12027, https://doi.org/10.1016/j.ceramint.2021.01.045.
[33] A. Elkoro, I. Casanova, 3D printing of structured nanotitania catalysts: a novel binder-free and low-temperature chemical sintering method, 3D Print. Addit. Manuf. 5 (2018) 220–226, https://doi.org/10.1089/3dp.2017.0164.
[34] A.D. McQueen, M.L. Ballentine, L.R. May, C.H. Laber, A. Das, M.J. Bortner, A. J. Kennedy, Photocatalytic degradation of polycyclic aromatic hydrocarbons in water by 3D printed TiO2 composites, ACS EST Water 2 (2021) 137–147.
[35] M.A. Ávila-López, J. Bonilla-Cruz, J. Méndez-Nonell, T.E. Lara-Ceniceros, Strong and lightweight stereolithographically 3D-printed polymer nanocomposites with low friction and high toughness, Polym. (Basel) 14 (2022), https://doi.org/10.3390/polym14173628.
[36] D.A. Kozlov, S.A. Tikhonova, P.V. Evdokimov, V.I. Putlyaev, A.V. Garshev, Stereolithography 3D printing from suspensions containing titanium dioxide, Russ. J. Inorg. Chem. 65 (2020) 1958–1964, https://doi.org/10.1134/S0036023620120098.
[37] S. Mubarak, D. Dhamodharan, N. Divakaran, M.B. Kale, T. Senthil, L. Wu, J. Wang, Enhanced mechanical and thermal properties of stereolithography 3d printed structures by the effects of incorporated controllably annealed anatase TiO2 nanoparticles, Nanomaterials 10 (2020), https://doi.org/10.3390/nano10010079.
[38] A. Vyatskikh, A. Kudo, S. Delalande, J.R. Greer, Additive manufacturing of polymer-derived titania for one-step solar water purification, Mater. Today Commun. 15 (2018) 288–293, https://doi.org/10.1016/j.mtcomm.2018.02.010.
[39] A. Purabgola, N. Mayilswamy, B. Kandasubramanian, Graphene-based TiO2 composites for photocatalysis & environmental remediation: synthesis and progress, Environ. Sci. Pollut. Res. 29 (2022) 32305–32325.
[40] Y. Zhao, L. Zhu, Y. Yu, F. Gao, W. Wang, D. Chen, X. Zhao, Facile one-pot preparation of Ti3+, N co-doping TiO2 nanotube arrays and enhanced photodegradation activities by tuning tube lengths and diameters, Catal. Today 355 (2020) 563–572.
[41] U. Bellè, F. Pelizzari, A. Lucotti, C. Castiglioni, M. Ormellese, M. Pedeferri, M. V. Diamanti, Immobilized nano-tio2 photocatalysts for the degradation of three organic dyes in single and multi-dye solutions, Coatings 10 (2020) 919.
[42] Y. Liu, J.H. Campbell, O. Stein, L. Jiang, J. Hund, Y. Lu, Deformation behavior of foam laser targets fabricated by two-photon polymerization, Nanomaterials 8 (2018), https://doi.org/10.3390/nano8070498.
[43] Z. Chen, J. Li, C. Liu, Y. Liu, J. Zhu, C. Lao, Preparation of high solid loading and low viscosity ceramic slurries for photopolymerization-based 3D printing, Ceram. Int. 45 (2019) 11549–11557, https://doi.org/10.1016/j.ceramint.2019.03.024.
[44] M. Schwentenwein, J. Homa, Additive manufacturing of dense alumina ceramics, Int. J. Appl. Ceram. Technol. 12 (2015) 1–7, https://doi.org/10.1111/ijac.12319.
[45] J. Bennett, Measuring UV curing parameters of commercial photopolymers used in additive manufacturing, Addit. Manuf. 18 (2017) 203–212, https://doi.org/10.1016/j.addma.2017.10.009.
[46] O. Guillaume, M.A. Geven, C.M. Sprecher, V.A. Stadelmann, D.W. Grijpma, T. T. Tang, L. Qin, Y. Lai, M. Alini, J.D. de Bruijn, H. Yuan, R.G. Richards, D. Eglin, Surface-enrichment with hydroxyapatite nanoparticles in stereolithography-fabricated composite polymer scaffolds promotes bone repair, Acta Biomater. 54 (2017) 386–398, https://doi.org/10.1016/j.actbio.2017.03.006.
[47] S. Zakeri, M. Vippola, E. Levänen, A comprehensive review of the photopolymerization of ceramic resins used in stereolithography, Addit. Manuf. 35 (2020), 101177, https://doi.org/10.1016/j.addma.2020.101177.
[48] L.A. Gonzàles-Burgiaga, M.N. Cynthia, M.M. Morones-esquivel, M. Avila-santos, A. Lemus-santana, B. Proal-n, Characterization and Comparative Performance of TiO2 Photocatalysts on 6-Mercaptopurine Degradation by Solar Heterogeneous Photocatalysis, Catalysts 10 (2020) 118.
[49] J. Bustillos, D. Montero-Zambrano, A. Loganathan, B. Boesl, A. Agarwal, Stereolithography-based 3D printed photosensitive polymer/boron nitride nanoplatelets composites, Polym. Compos. 40 (2019) 379–388, https://doi.org/10.1002/pc.24662.
[50] B. Hill, T. Roger, F.W. Vorhagen, Comparative analysis of the quantization of color spaces on the basis of the CIELAB color-difference formula, ACM Trans. Graph. 16 (1997) 109–154.